IEEE Robotics and Automation Letters (RA-L) paper, presented at ICRA 2026, Vienna, Austria. Cite as RA-L paper.

Design of a Passive Gravity Compensation Mechanism for Wearable Bilateral Lower Limb Exoskeletons

Tongshu Chen, Ke Shi, Maozeng Zhang, and Aiguo Song, *Senior Member, IEEE*

***Abstract*—Gravity compensation has been widely employed in lower limb exoskeletons to reduce leg load and alleviate muscle fatigue. Passive compensation approaches offer inherent safety and lightweight advantages; however, existing designs are often constrained by the bulk and complexity of spring-based mechanisms, which compromises the compactness and reliability of the exoskeleton. To address these limitations, a gravity compensation mechanism is developed for a wearable passive bilateral lower limb exoskeleton, featuring a compact, simple, and robust design. A unilateral compensation concept based on a synthetic centroid mapping method is first introduced and then extended to a bilateral configuration through a differential structure. Combined with an adaptive constant-force mechanism, the resulting system maintains structural simplicity and spatial efficiency, making it suitable for wearable applications with limited integration space. An exoskeleton prototype is constructed based on the proposed mechanism, and its performance is evaluated through experiments. The results demonstrate that the proposed system effectively compensates for leg weight during walking while maintaining a lightweight, low-complexity, and structurally robust design.**

***Index Terms*—Gravity compensation unit, differential mechanism, walking assistance, passive lower limb exoskeleton.**

I. Introduction

LOWER limb exoskeletons are used for human movement assistance and rehabilitation [1]. They can improve the motor abilities of healthy individuals or serve as a rehabilitation tool for patients with limb pathologies [2]. Lower limb exoskeleton can be classified into active and passive types [3]. Active exoskeletons typically incorporate actuators and energy supply device to actively drive movement of the limb. These systems must overcome both the weight of the limb and the exoskeleton, which results in high power demands and may compromise the safety of human-robot interaction [4]. In contrast, passive exoskeletons can assist the limb movement by using gravity compensation (GC) mechanism, which makes actuators unnecessary and ensures safer human-robot interaction. Passive exoskeletons also have the inherent advantage of the lightweight and flexible structure due to the unnecessary use of actuators.

The passive GC mechanisms in exoskeletons typically consist of two types: counterweights and spring-based mechanisms. The primary distinction between these mechanisms lies in the form of energy conversion [5]. The counterweight-based mechanism utilizes the mass of the weights to achieve gravitational balance [6], [7]. Although simple and effective, this approach significantly increases the system's mass and inertia. The spring-based mechanism can store elastic potential energy to maintain system balance. Due to their compactness and lightweight characteristics, spring-based mechanisms are widely adopted in passive exoskeleton designs [8].

Spring-based GC for multi-DoF robotic systems can be achieved by strategically combining multiple one-DoF units, which are widely used due to their structural simplicity and stability [9], [10]. Depending on their motion characteristics, one-DoF units are typically categorized into constant-force mechanisms and one-DoF rotational joints. The former is commonly used for linear motion compensation, with representative implementations found in [11], [12], while the latter is suited for rotational motion, as demonstrated in [13], [14]. Cho et al. proposed a space mapping method for the analysis and design of GC mechanisms for multi-DoF manipulators, employing one-DoF GC units as fundamental components [10]. This method has been adopted in subsequent studies, including [8] and [15]. However, as the DoF increases, the complexity of the structure escalates, which may restrict the practical implementation [15]. Consequently, for multi-DoF systems, reducing the number of springs through mechanical optimization has become an other strategy for achieving gravity balance. This approach enables effective GC while reducing overall system complexity [9]. Smith et al. proposed a four-DoF exoskeleton system that achieves perfect GC by employing a spring redistribution strategy [16]. This method utilizes two springs to compensate for a three-DoF rotational joint and a single-DoF rotational joint. In a comparable configuration, Agrawal et al. [17] proposed a GC unit using auxiliary links and two springs to achieve the spatial balance of the system. Building upon this, Lin et al. proposed an alternative arrangement of two springs without using auxiliary links, yet still requiring the identification of the centroid [18].

Based on the aforementioned GC mechanisms, many passive lower limb exoskeletons have been developed. Agrawal et al. proposed a gravity-balancing leg orthosis that constructs the center of mass using auxiliary links [17]. The system

Received 10 May 2025; accepted 29 November 2025. Date of publication 15 December 2025; date of current version 22 December 2025. This article was recommended for publication by Associate Editor M. Kim and Editor H. Yu upon evaluation of the reviewers' comments. This work was supported in part by the Jiangsu Key Research and Development Plan under Grant BE2023023-1, in part by the Natural Science Foundation of Jiangsu Province Major Project under Grant BK20232008, and in part by the Fundamental Research Funds for the Central Universities. *(Corresponding author: Aiguo Song.)*

This work involved human subjects or animals in its research. Approval of all ethical and experimental procedures and protocols was granted by the Clinical Research Ethics Committee of Zhongda Hospital under Application No. 2022ZDSYLL397-P01, and performed in line with the Declaration of Helsinki.

The authors are with the School of Instrument Science and Engineering, Southeast University, Nanjing 210096, China (e-mail: t.s.chen@seu.edu.cn; shike307@gmail.com; mzzhang@seu.edu.cn; a.g.song@seu.edu.cn).

Digital Object Identifier 10.1109/LRA.2025.3644149

IEEE Robotics and Automation Letters (RA-L) paper, presented at ICRA 2026, Vienna, Austria. Cite as RA-L paper.

employs two springs connected to a determined center of mass, forming a multi-DoF GC unit for a planar two-link mechanism. Shi et al. used cams to construct two one-DoF GC units to counteract the mass of the lower limbs [19]. Bai et al. designed a lower limb exoskeleton using planetary-gear-based GC units to compensate for the mass of the lower limb [20]. Due to the need for both compression and tension springs in the mechanism, the exoskeleton only utilizes tension springs as an approximation for GC. Such approximate compensations have also been explored in other works. Alamdari et al. proposed an approximate balance mechanism for leg orthosis using zero-free-length springs [21].

As previously reported, numerous GC mechanisms have been developed for lower limb exoskeletons. However, due to the complexity of multi-joint compensation in the lower extremities, these systems typically rely on multiple springs to achieve perfect compensation across multiple DoF. This multi-spring approach significantly increases the system's mechanical complexity. The integration, adjustment, and pre-tensioning of these springs also pose substantial challenges in structural design and performance optimization. Moreover, most of these designs necessitate the use of zero-free-length springs, thus introducing additional structural complexity. This inevitably compromises the overall simplicity, compactness, and practical deployability of the system.

To address the aforementioned issues, this study presents a multi-DoF GC unit with differential mechanism (D-GCU) utilizing a single spring, designed for bilateral lower limb GC. The D-GCU allowing it to simultaneously provide GC for both lower limbs. Additionally, the use of a single spring simplifies the installation and adjustment of the system significantly. A prototype of the passive bilateral lower limb exoskeleton with the D-GCU has been fabricated, and corresponding experiments have been conducted to assess its practical performance. The main contributions of this study are as follows:

- A novel GC mechanism based on synthetic centroid mapping is proposed and extended to a bilateral four-DoF configuration using a differential design.
- A compact and wearable bilateral lower limb exoskeleton is developed, integrating a single-spring constant-force unit to achieve multi-DoF gravity compensation.
- An exoskeleton prototype is developed and experimentally validated, demonstrating effective load reduction on both limbs and the device during assisted walking.

In the rest of this study, Section II analyzes the lower limb motion model and proposes the design principles of the GC unit based on the centroid method, as well as the design of the D-GCU for bilateral lower limb compensation. Section III introduces the prototype design of a wearable passive bilateral lower limb exoskeleton with D-GCU. Section IV conducts the experiments for evaluating the practical performance of the exoskeleton prototype and the usability of the exoskeleton is verified. Section V discusses the limitation of the proposed exoskeleton with D-GCU and concludes this study.

II. Mechanical Analysis

As outlined in Section I, this study presents an in-depth analysis and design of the D-GCU for lower limb compensation. This section begins by proposing an innovative design of the GC unit for unilateral lower limb compensation based on the centroid method. By analyzing the centroid position, the operational principle of the GC unit is outlined. Subsequently, combining the principle of the unilateral GC unit with the bilateral symmetry of the lower limbs, the design and analysis of the single-spring-based D-GCU for bilateral lower limbs compensation are discussed.

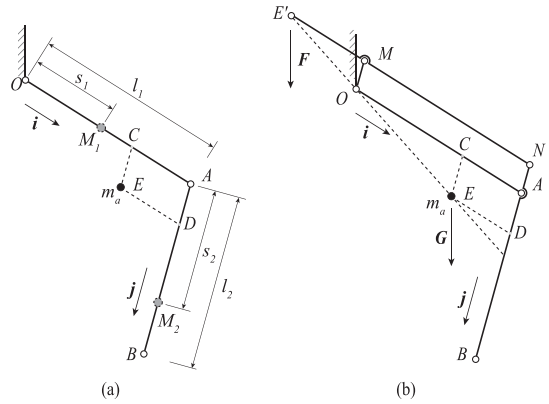

Fig. 1. (a) The simplified model of the lower limb. (b) Principle of lower limb GC unit.

A. Design Principles of the GC Unit for Unilateral Lower Limb Compensation

The analysis of lower limb motion is essential for the design of exoskeletons. In the analysis of human motion, the human body can be divided into three planes: sagittal, coronal, and horizontal planes [22]. The sagittal plane is the dominant plane where most of the motion of lower limb takes place. Therefore, in the design of lower limb exoskeletons, the lower limb is commonly approximated as a planar two-link mechanism to simplify the analysis and design process [23]. The ankle joint is typically not considered due to its limited range of motion [17].

The centroid method is widely applied in the design of GC unit for two-link mechanisms [17], [18], [21]. However, most GC unit designs of them employ multiple springs to achieve system balance, which can adversely affect the reliability and robustness of the exoskeleton system [16]. Therefore, this section first derives the centroidal motion characteristics and, based on these, a single-spring multi-DoF GC unit is proposed for the unilateral lower limb compensation. The simplified model of the lower limb is shown in Fig. 1(a). The hip and knee joints are represented by points O and A, respectively. The links OA and AB represent the thigh and the shank, and the foot is approximated as point B at the end of the shank. The mass of the thigh, shank, and foot are approximated as point mass M_1 with mass m_1 and point mass M_2 with mass m_2, where point mass M_2 also includes the weight of the foot. By taking point O as the origin of the plane coordinate system, the position vectors of the centroids for the thigh and shank can be written as

$$\begin{aligned} \vec{r_1} &= s_1\vec{i} \\ \vec{r_2} &= l_1\vec{i} + s_2\vec{j} \end{aligned} \tag{1}$$

where l_i (i=1, 2) denotes the lengths of each link, s_1 denotes the distance of the point mass M_1 to hip joint O, s_2 denotes the distance of the point mass M_2 to knee joint A, $\vec{r_i}$ (i=1, 2) denotes the position vector of m_i, and $\vec{i}$, $\vec{j}$, denotes the unit vectors along the rods OA and AB. According to the centroid

IEEE Robotics and Automation Letters (RA-L) paper, presented at ICRA 2026, Vienna, Austria. Cite as RA-L paper.

synthesis formula, the position vector of the composite centroid $\vec{r_a}$ of the lower limb can be written as

$$\vec{r_a} = \sum_{i=1}^{2} m_i \vec{r_i} / \sum_{i=1}^{2} m_i = \left(\frac{m_1 s_1 + m_2 l_1}{m_a} \right) \vec{i} + \frac{m_2 s_2}{m_a} \vec{j}$$

$$m_a = \sum_{i=1}^{2} m_i = m_1 + m_2 \tag{2}$$

When the system is determined, m_i, s_1, l_i, i=1, 2, are constant. Therefore, the position vector of the composite centroid $\vec{r_a}$ of the lower limb can be determined by fixed-length vectors of $\vec{i}$ and $\vec{j}$. In order to facilitate the analysis of the characteristics of synthesized centroid, virtual links CE and ED are introduced, which are parallel to links AB and OA, respectively, and satisfy the following conditions:

$$|OC| = \frac{m_1 s_1 + m_2 l_1}{m_a}$$

$$|ED| = \frac{m_2 s_2}{m_a} \tag{3}$$

Thus, the centroid can be determined by the intersection point E of the virtual links.

Due to the centroidal characteristics of the planar two-link model, a single-spring GC unit for the lower limb was designed based on the parallel four-bar mechanism. The principle of lower limb GC unit is shown in Fig. 1(b). Based on the existing two-link mechanism, a set of parallel links $OANM$ is introduced, where MN is parallel to OA and OM is parallel to AB. Let $k = \frac{OM}{CE}$, and extend the link MN in the reverse direction to point E', ensuring that the length of link $E'M$ satisfies $|E'M| = k|OC|$. Hence, the position vector $\vec{r'}$ of point E' can be written as

$$\begin{aligned} \vec{r'} &= -k\,|CE|\,\vec{j} - k\,|OC|\,\vec{i} \\ &= -k \left(\frac{m_1 s_1 + m_2 l_1}{m_a} \vec{i} + \frac{m_2 s_2}{m_a} \vec{j} \right) = -k\vec{r_a} \end{aligned} \tag{4}$$

Therefore, point E', O and E are collinear, and the relationship $|OE'| = k|OE|$ holds. This can be interpreted as a virtual lever with a constant lever arm ratio and variable length. In the virtual lever, point O acts as the fulcrum and point E represents the centroid which experiences a vertically downward gravitational force $\vec{G}$.

Based on the lever equilibrium condition, it can be deduced that applying a constant force $\vec{F} = \vec{G}/k$ at point E' will maintain system balance, with k being the constant ratio of the lever arm lengths. In the actual design process, k is treated as a design parameter, selected by considering both the linkage lengths and the target constant force. The proposed GC unit includes a constant force mechanism (CFM) and adaptive links to keep the virtual lever balance. To facilitate the explanation, point E' is referred as the centroid mapping point. The compensatory force $\vec{F}$ is generated by a constant-force mechanism, most commonly realized through a single-spring configuration due to its simplicity and ease of integration [13]. A set of adaptive links is employed to transmit the force to the centroid mapping point and accommodate its swinging motion in the sagittal plane. The working principle will be discussed in detail in Section II-B. Through the action of the GC unit, the unilateral lower limb system can achieve balance at any position within the activities of daily living range.

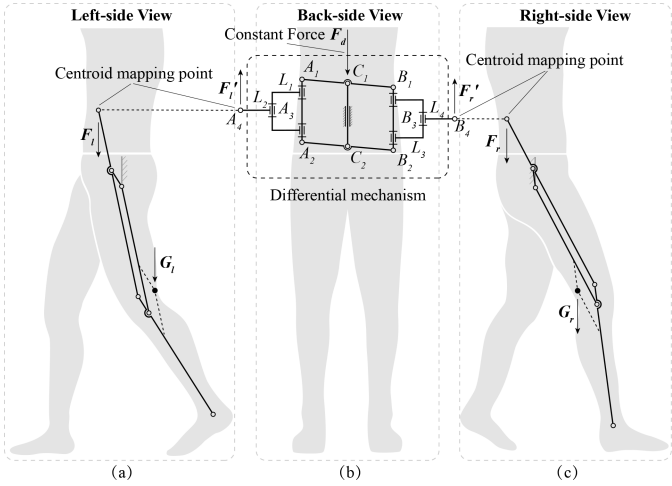

Fig. 2. Schematic diagram of the D-GCU mechanism. (a) Left-side linkage view. (b) Differential mechanism (back view). (c) Right-side linkage view.

B. Design Principles of D-GCU for Bilateral Lower Limb Compensation

In this section, the application of the proposed GC unit in bilateral lower limb compensation will be discussed, as well as the design and analysis of the D-GCU.

Through the analysis of the required force, it is concluded that the force provided by the CFM depends on the compensated mass and the lengths of the parallel four-bar mechanism. This implies that when the parameters of the bilateral lower limb compensation mechanisms are identical, the required force remains consistent. On the other hand, the movements of the bilateral lower limbs are relatively independent, meaning that the swinging motion of the centroid mapping points in the sagittal plane is not correlated. Therefore, for bilateral lower limbs, two independent GC units can be used to provide compensation for each limb separately. Such a configuration is feasible but somewhat redundant. Thus, based on the required force and motion characteristics of the centroid mapping point described above, a D-GCU is further proposed for compensating both lower limbs.

The D-GCU mainly consists of a CFM, a differential mechanism, and a set of links on both sides of the lower limbs. The working principle of D-GCU is shown in Fig. 2. The CFM, composed of a single spring, generates a force of $\vec{F_d} = 2\vec{F_l} = 2\vec{F_r}$, which is then evenly distributed to the centroid mapping points on both sides via the differential mechanism. This differential mechanism not only ensures even force distribution but also accommodates the movement of the centroid mapping points. In the sagittal plane, the swinging motion of the centroid mapping point can be decomposed into displacements in both the vertical and horizontal directions. Therefore, differential mechanism's adaptability will primarily focus on accommodating these two types of displacement.

As seen in the back-side view of Fig. 2, the structure of the differential mechanism is comprised of two key components that respectively facilitate adaptation to vertical and horizontal

IEEE Robotics and Automation Letters (RA-L) paper, presented at ICRA 2026, Vienna, Austria. Cite as RA-L paper.

plane movements, as well as facilitate equal distribution of forces. Initially, a set of parallelogram linkages $A_1A_2B_1B_2$ is employed, which move within the coronal plane. The midpoints of links A_1B_1 and A_2B_2 are hinged via links C_1C_2, allowing the parallelogram linkage to translate vertically within the coronal plane. The rotation of the parallelogram linkage permits the vertical height discrepancy between links A_1A_2 and B_1B_2, accommodating the height differences of the centroid mapping points on both sides during motion. Constrained by the vertically oriented link C_1C_2, the parallelogram linkage ensures that the links A_1A_2 and B_1B_2 remain vertical during rotation. This ensures that the second part of the differential mechanism, comprising the two-bar linkages L_1L_2 and L_3L_4 which located on either side of the parallelogram linkage, will always operate within the horizontal plane. The left-side two-bar linkage L_1L_2 rotates around link A_1A_2, with bar L_2 rotating relative to L_1 at the hinge point A_3. The terminal point A_4 of the link L_2 is fixed to the centroid mapping point of the left lower limb, enabling horizontal two-bar linkage motion to accommodate the displacement in the anterior-posterior direction during motion. Additionally, the coupling displacements generated in the left-right direction during the rotation of the parallelogram linkage are also accommodated by the two-bar linkages. The right-side two-bar linkage L_3L_4 operates similarly to the left side. The equal distribution of the constant force at the centroid mapping points also relies on these two components. The bilateral two-bar linkages ensure that the vertical forces generated at any centroid mapping point position are transmitted to links A_1A_2 and B_1B_2 with invariant magnitude. The parallelogram linkages $A_1A_2B_1B_2$, leveraging the principle of moments, guarantee that the constant force applied at its center is stably and equally distributed to links A_1A_2 and B_1B_2, thereby maintaining force equilibrium. Through these two mechanisms, the output of the CFM is transmitted to both lower limbs, providing the required motion adaptation and achieving gravity balance for the system. In scenarios where unilateral compensation is required, it can be achieved by taking half of the differential mechanism along the link C_1C_2 and replacing the parallelogram linkage of the differential mechanism with a rigid, non-rotatable frame.

III. Prototype Design

Based on the analysis, the design principles of D-GCU for bilateral lower limb compensation were presented in Section II. This section will introduce the prototype design of a wearable passive bilateral lower limb exoskeleton with D-GCU. The mechanical designs of lower limb linkages, CFM and differential mechanism, which are the three components of the prototype, will be presented in sequence.

An overview of the exoskeleton system is demonstrated in Fig. 3(a). The prototype is mainly made of aluminum and carbon fiber. Its weight is about 5.3 kg. The exoskeleton system mainly consists of three components: lower limb linkages, CFM and differential mechanism. The exoskeleton is worn on the back through the upper body harness, which fixes the base of the exoskeleton to the body, while lower limb linkages are secured to the bilateral lower limbs using straps. The upper body harness is fixed at the shoulders and waist, ensuring the stability of the exoskeleton during wear.

During the mechanical design of the exoskeleton prototype, due to the inability to directly connect the linkages to the bones of the leg, a set of lightweight lower limb linkages was designed to be worn on the outside of the lower limbs, as shown in Fig. 3(c).

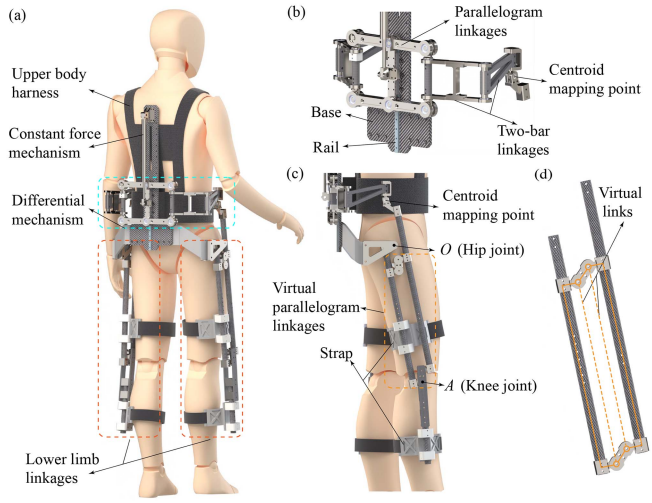

Fig. 3. (a) Overview of the wearable passive bilateral lower limb exoskeleton with D-GCU. (b) The detailed view of the differential mechanism. (c) The detailed view of lower limb linkages. (d) The detailed view of virtual parallelogram linkages.

TABLE I
Design Parameters of the Proposed Passive Exoskeleton

Parameter	Value / Description
Total device mass	5.3 kg
Degree of freedom	4
Constant force	600 N
Range of motion (joint O)	$0 \sim 110$ deg
Range of motion (joint A)	$0 \sim 120$ deg

At this point, the lower limb centroid motion plane and the plane of the lightweight linkages are parallel to each other. The offset between the centroid and the lightweight linkages remains constant, thereby generating a constant torque that is parallel to the plane of the linkage. However, the lower limb linkages exhibit only rotational freedom within the plane, meaning that the torque cannot perform work to induce a change in the system's energy. Consequently, the structure of the offset linkage remains applicable to the compensation method based on the centroid mapping. Furthermore, the mass rod model established for deriving the centroid mapping point position previously considered only the mass of the lower limbs. To refine the system model and enhance its accuracy, the mass of the lower limb linkages can be incorporated into the computational framework, enabling the determination of a hybrid centroid mapping point for both the exoskeleton and the human body. Design parameters of the proposed passive exoskeleton is depicted in the Table I.

Studies examining activities of daily living have indicated that, within the sagittal plane, the required joint angles for effective movement are 80 deg of hip flexion and 110 deg of knee flexion [24], [25]. Therefore, the motion ranges of the designed exoskeleton are about 110 deg in flexion for the hip joint, and about 120 deg in flexion for the knee joint, which cover the required motion ranges of the lower limbs during activities of daily living.

As shown in the Fig. 3(c), the offset lower limb linkages consists of a set of virtual parallelogram linkages. The lower limb linkages have two rotational DoFs, located at joints O and A, respectively. The rotation axis at joint O corresponds to the

IEEE Robotics and Automation Letters (RA-L) paper, presented at ICRA 2026, Vienna, Austria. Cite as RA-L paper.

hip joint, with its projection in the sagittal plane overlapping. Similarly, the rotation axis at joint A corresponds to the knee joint, and its projection in the sagittal plane also coincides. The lower limb linkage are hinged to the base at joint O, while at the centroid mapping point, a two-DoF rotational mechanism is used to establish a spatial connection between the lower limb linkages and the differential mechanism. To accommodate the upright posture of the lower limbs, a configuration based on virtual parallelogram linkages was employed, enabling the lower limb linkages to fully extend and align in parallel. As shown in Fig. 3(d), the virtual parallelogram linkages make use of virtual links to prevent collisions caused by overlapping components in conventional parallelogram mechanisms, allowing a greater range of motion.

Constant force devices can be implemented in a variety of ways [11], [12], each capable of delivering a constant force over a defined displacement. In the designed wearable passive exoskeleton, gas springs (E-FHL76), which feature a 180 mm stroke and deliver a constant force of 600 N, are employed to provide the constant force, due to their ability to accommodate longer operational ranges and their structural simplicity. Based on actual measurements, the gas spring can achieve an error margin of $\pm 10\%$ within the effective stroke range. Gas springs are characterized by their lightweight nature, high output force, and ease of installation [26].

A detailed view of the differential mechanism is demonstrated in Fig. 3(b). The differential mechanism is composed of a set of parallelogram linkages and two pairs of two-bar linkages. The parallel linkage mechanism is rigidly connected to a sliding block, which is able to move vertically along a slide rail installed on the base. A connector for a gas spring is attached to the parallelogram linkages, allowing the constant force generated by the gas spring to act on the differential mechanism. The other end of the gas spring is anchored to the base. The two-bar linkage system consists of links that can rotate about two vertical axes. One end of the linkage connects to the vertical link of the parallelogram and rotates around it, while the other end connects to the centroid mapping point through a two-DoF rotational mechanism. This differential mechanism is symmetric on both sides, enabling independent swing of the centroid mapping points in sagittal plane while distributing the constant force evenly across both lower limbs.

IV. Experiments

In this study, the wearable passive bilateral lower limb exoskeleton with D-GCU is proposed for passive potential applications. In this system, the exoskeleton compensates for the weight of both the lower limbs and the exoskeleton itself, allowing the user to overcome only the additional forces arising from dynamics and compensation errors during movement. However, in practical applications, the compensation performance of the D-GCU may be affected by factors such as dynamic effects, friction, mechanical errors, and inaccuracies in estimating limb parameters. Therefore, a prototype of the bilateral lower limb exoskeleton was designed and several experiments were conducted to evaluate its actual performance.

A. Experimental Setup

The prototype of the exoskeleton and the testing system are illustrated in Fig. 4. Ten healthy subjects (7 males and 3 females, age 26 ± 4 years, weight 65 ± 10 kg, height 175 ± 8 cm) were recruited for this experiment. To evaluate the exoskeleton's compensation performance for the subjects' lower limbs during walking, four force/torque sensors (Mini45, ATI, North Carolina, USA) were employed to measure the assistive forces provided by the exoskeleton. These ATI sensors were symmetrically installed at the connection points between the exoskeleton and the subjects' thigh and shank. Additionally, two sets of inertial measurement units (HI221 IMUs, Hipnuc, Beijing, China) were positioned on the lower limb linkages of the exoskeleton. During the experiment, the subjects wore the lower limb exoskeleton and performed walking movements. The IMUs recorded the rotational angles of the knee and hip joints, while the force/torque sensors measured the assistive forces exerted by the exoskeleton. The recorded forces were then converted into the corresponding assistive torques at the knee and hip joints based on static force analysis. Theoretically, in an ideal D-GCU system, the actually required joint torques during walking should approach zero. However, in practical applications, dynamic effects and compensation errors may result in higher actually required joint torques. Therefore, the performance of the D-GCU can be evaluated by comparing the actually required joint torques while wearing the exoskeleton with the theoretically required joint torques calculated without the exoskeleton.

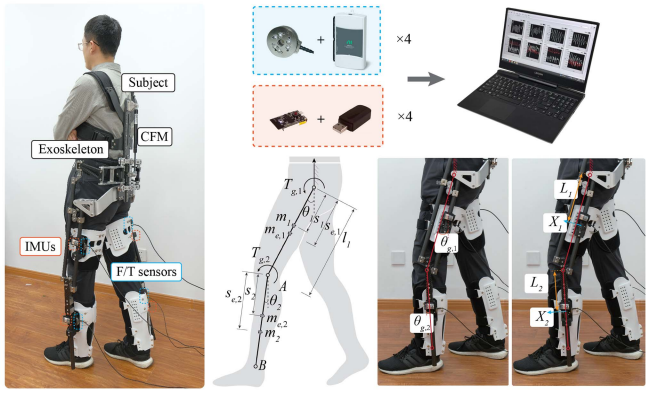

Fig. 4. The exoskeleton's prototype and test system.

The experiment aimed to assess the exoskeleton's real-world performance during walking, focusing on lower limb assistance and verifying bilateral compensation via the differential mechanism. During the experiment, the subjects wore the exoskeleton and walked on a treadmill (WP-001, JD, Beijing, China) at a speed of 0.9 m/s for one minute. Joint angle and force data from both lower limbs were recorded and analyzed. Under these experimental conditions, joint angle and force data of every subjects were collected for 20 gait cycles to ensure the reliability and reproducibility of the results.

To better assess the specific impact of the exoskeleton's assistance on walking, electromyography (EMG) signals, which reflect the active torques generated by the subjects, were collected and analyzed using EMG equipment (Trigno, Delsys Incorporated, Natick, USA). With exoskeleton assistance, the active torques required from the relevant muscles during walking is reduced, which is reflected as a decrease in the EMG signal. EMG electrodes (Delsys) were placed on the bilateral rectus femoris (RF), biceps femoris (BF), tibialis anterior (TA), and gastrocnemius (GA) to assess muscle activation [27]. The study was reviewed and approved by the Ethics Committee.

IEEE Robotics and Automation Letters (RA-L) paper, presented at ICRA 2026, Vienna, Austria. Cite as RA-L paper.

B. Data Processing

Based on the lower limb and exoskeleton parameter model presented in Fig. 4, the gravitational torques acting at the hip joint $T_{g,1}$ and the knee joint $T_{g,2}$, which correspond to the theoretically required joint torques for gravity compensation, can be formulated as

$$\begin{aligned} T_{g,2} &= m_2 s_2 g sin\theta_2 + m_{e,2} s_{e,2} g sin\theta_2 \\ T_{g,1} &= T_{g,2} + (m_1 s_1 + m_{e,1} s_{e,1}) g sin\theta_1 \\ &\quad + (m_2 + m_{e,2}) l_1 g sin\theta_2 \end{aligned} \tag{5}$$

where $m_{e,i}$ (i=1, 2) denotes the mass of the exoskeleton at the thigh and shank segments. $s_{e,1}$ denotes the distance between the center of mass of the thigh exoskeleton and the hip joint. $s_{e,2}$ denotes the distance between the the center of mass of the shank exoskeleton and the knee joint. θ_1 and θ_2 represent the absolute angles of the hip and knee joints relative to the vertical direction, respectively.

The primary data collected during the experiment include joint angles and the assistive forces from the exoskeleton. $\theta_g, 1$ and $\theta_g, 2$ represent the absolute angles of the joints relative to the vertical direction, as measured by the IMUs. $\vec{X}_i$ (for i=1,2) denote the components of the forces measured by the force/torque sensors in the sagittal plane, which are perpendicular to the corresponding links. The assistive torques at the hip $T_{a,1}$ and knee $T_{a,2}$ joint can be calculated using the following expressions

$$\begin{aligned} T_{a,2} &= X_2 L_2 \\ T_{a,1} &= X_2(cos(\theta_{g,1} - \theta_{g,2}) l_1 + L_2) + X_1 L_1 \end{aligned} \tag{6}$$

where L_i (i=1, 2) denotes lever arm between the force sensor and the corresponding joint.

By further processing the actually and theoretically required joint torques, we performed a statistical analysis across all subjects using the absolute torque values, focusing primarily on two key parameters

- Peak Torque Index (PTI): The normalized value of the average peak joint torque within 20 gait cycles.
- Mean Torque Index (MTI): The normalized value of the average joint torque within 20 gait cycles.

To eliminate the torque variations caused by inter-subject differences, the joint torque data for each subject were normalized based on the maximum absolute joint torque across all 20 gait cycle, enabling subsequent statistical analysis. These two parameters assess the compensation performance from two aspects: the PTI indicates how well the system compensates under the most demanding postures, while the MTI reflects the overall effectiveness throughout the gait cycle. A statistical t-test was performed on the required joint torques with and without exoskeleton assistance, and the reduction ratio was computed to more explicitly illustrate the compensation capability [8]. The normality and homogeneity of variance assumptions were assessed using the Shapiro-Wilk test and Levene's test, respectively. The results of both tests indicate that the data met both assumptions.

In terms of EMG data processing, subjects performed an maximum voluntary contraction (MVC) procedure to normalize EMG signals to %MVC. Muscular effort during walking, with and without the exoskeleton, was quantified by calculating the root mean square (RMS) of the %MVC data for each gait cycle. Based on the obtained data, we performed t-tests on %MVC data with and without exoskeleton to analyze the actual effect of the exoskeleton on walking assistance.

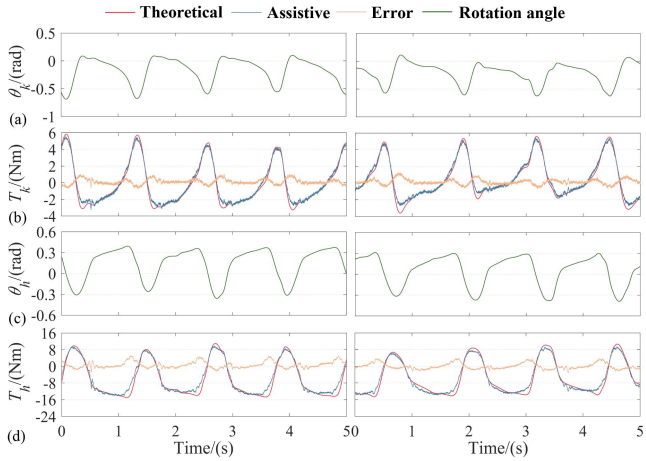

Fig. 5. The experimental result from a single walking trial. The left and right sides correspond to the data of the left and right legs, respectively. (a) and (c) illustrate the rotation angle at the knee joint and hip joint. (b) and (d) illustrate the theoretically required joint torques calculated without the exoskeleton, the assistive torque provided by the exoskeleton, and the compensation error at the knee joint and hip joint.

C. Results

The joint angle as well as the joint torque during a single walking trial are depicted in Fig. 5. This set of figures illustrate the data of the actually required joint torques in both lower limbs, along with the theoretically required joint torques without D-GCU, thereby demonstrating the compensation effect. Throughout the experiment, both legs received the corresponding assistive torques provided by the system, validating the effectiveness of the differential mechanism. As shown in Fig. 5(b) and (d), the mass of the lower limb was effectively compensated. The assistive torque provided by the system closely aligns with the theoretically required torque of the lower limbs, with minor discrepancies. On one hand, the compensation performance of the exoskeleton is influenced by the linkage parameters, which are determined based on estimations of lower limb parameters. Errors in these estimations structurally impact the effectiveness of the compensation. On the other hand, despite the integration of multiple bearings and other components to reduce friction, inherent friction in the gas springs, as well as in the guide rails and sliders, imposes certain limitations on the system's compensation performance. Additionally, misalignment between the exoskeleton and the subjects' lower limbs introduces deviations in force transmission, further affecting the overall compensation efficacy. In most gait cycles, the assistive torque is lower than the theoretical required joint torque without GC due to the influence of friction. However, in certain specific postures, the dominance of friction and compensation errors may lead to assistive torque exceeding the theoretical required joint torque without GC. This issue mainly occurs near singular configurations but is rare and limited to postures with minimal torque demand. The resulting overcompensation is negligible and does not compromise the system's overall robustness in practical use.

Fig. 6 depicts the PTI and MTI at the knee and hip joints across ten subjects. Based on the PTI and MTI statistics, it is evident that

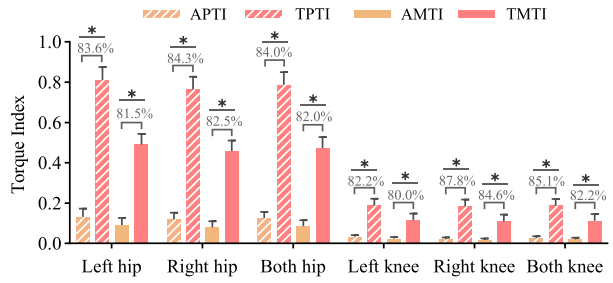

Fig. 6. The PTI and MTI with their corresponding reduction ratios at the hip and knee joints from ten subjects. APTI and TPTI denote the PTI of actually and theoretically required joint torque, respectively. AMPI and TMPI denote the MTI of actually and theoretically required joint torque, respectively. Data are presented as mean ± standard deviation. Bars marked with asterisks indicate statistically significant differences ($p < 0.05$).

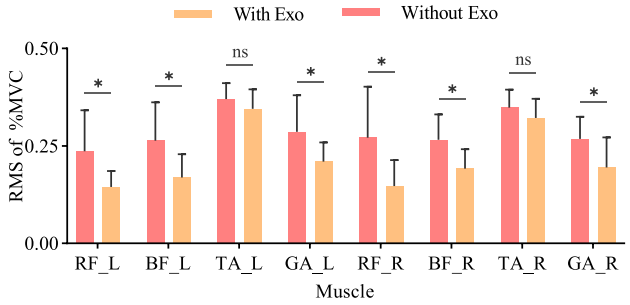

Fig. 7. RMS of %MVC data for the walking task. L and R indicate left and right muscles, respectively. Data are presented as mean ± standard deviation. Bars marked with asterisks indicate statistically significant differences ($p < 0.05$).

the system provides significant assistance during walking, as the required joint torques are significantly reduced. The reduction ratio in PTI was higher than that of the MTI, indicating that the system performs better in regions where higher assistive torques are required, while showing reduced effectiveness in low-torque phases. This observation further validates the phenomenon illustrated in Fig. 5. The compensation effects on both legs were comparable, confirming the bilateral symmetry of the assistive capability enabled by the differential mechanism. Additionally, all subjects reported a clear perception of the assistive force. However, three subjects mentioned suboptimal wearing comfort, noting that the limited hip joint mobility slightly affected their gait.

Fig. 7 depicts the RMS of %MVC data of leg muscles with and without exoskeleton assistance. Similar trends were observed in both legs: the RMS of %MVC data of RF, BF, and GA showed notable reductions, while the RMS of %MVC data of TA exhibited minimal change. This is primarily because TA contributes little to knee joint motion, and thus its activity was less affected by the exoskeleton. The experimental results were consistent with our expectations, demonstrating in practice that the system reduces walking effort and provides assistance to the lower limbs.

V. Discussion and Conclusion

The number of springs can serve as an indicative metric for the structural complexity of spring-based GC systems. Notably, multiple springs placed at the same location for stiffness enhancement are counted as one. Fewer springs typically lead to simpler designs with improved stability and reliability. Single-spring mechanisms are widely used in systems with limited compensation requirements but are generally restricted to single-joint applications and lack the capacity for spatial compensation. In contrast, multi-spring systems are capable of compensating for complex spatial motions. For instance, the Wilmington Robotic Exoskeleton employs two springs with parallelogram linkages to achieve four-DoF GC, though the number of effectively compensated DoFs is reduced [28]. Similarly, Shi et al. developed a four-DoF system using five springs to compensate for three joints [8], significantly increasing structural complexity. In multi-DoF GC systems, minimizing the number of springs significantly reduces structural complexity and enhances system stability. Compared to existing passive lower limb wearable exoskeletons [17], [20], [21], the proposed system features a compact and simplified design that utilizes a single spring to achieve bilateral GC. The design of the constant-force mechanism offers various implementation options [11], [12]. In this system, a gas spring is adopted due to its large stroke length, high force output, and ease of installation and replacement. Compensation for different system masses can be achieved by simply replacing the spring to satisfy the required output force. By mapping the centroid of the target system posteriorly using simple linkages, D-GCU enables GC without protruding structures on the limb segment, which facilitates integration for an active system.

The proposed passive exoskeleton system presents a practical and effective solution for assisting individuals with lower limb motor impairments in rehabilitation and daily mobility tasks. Its anthropomorphic joint configuration and compact design accommodate a wide range of daily activities. Moreover, actuators can be directly mounted at the hip and knee joints to provide additional assistance during movement. The inherent GC mechanism significantly reduces actuator power requirements, thereby minimizing the risk of injury. Utilizing low-power actuators with low gear reduction ratios further enhances safety and compliance in human–exoskeleton interaction. The proposed system focuses on assisting walking. In other gait scenarios, such as stair ascent and descent, it can also provide a certain degree of assistance to the limbs. However, these tasks primarily induce changes in the body's overall potential energy, which are substantially greater than the energy variations associated with limb motion. Such cases involve more complex mechanisms, fall beyond the scope of this study, and remain to be further explored.

Despite demonstrating promising performance, the system also presented some limitations. At present, the exoskeleton includes four degrees of freedom across both lower limbs. While these cover the major joints involved in daily activities, adding more DoFs especially at the hip joint could improve wearer comfort and reduce injury risks. Notably, the D-GCU mechanism is not restricted to four-DoF configurations; it is equally applicable to hip joints with higher degrees of freedom, enabling compensation for spatial motions. Future developments may incorporate additional DoFs to further improve overall usability and safety. Furthermore, according to the design derivation of the D-GCU, the linkage parameters of the compensation structure are dependent on the biomechanical characteristics of the limb being assisted. As the target system changes, the corresponding linkage parameters required for theoretical perfect balance must also be adjusted. Meanwhile, the output force of the gas spring cannot be continuously adjusted and is limited to discrete values,

which limits the system's overall adjustability. To address this, the exoskeleton is structurally designed to allow easy replacement of linkages, enabling adaptation to different users and load conditions.

Although the current prototype does not yet fully achieve the theoretical compensation performance due to friction and assembly tolerances, it still demonstrates a strong capability to counteract the gravitational load of both the limb and the exoskeleton. Compared to existing multi-DoF compensation systems [8], [19], [20], the proposed design exhibits comparable compensation performance, while maintaining a significantly simpler and more compact mechanical structure. These advantages highlight its strong potential for practical implementation in lower limb mobility assistance.

REFERENCES

[1] W. Huo, S. Mohammed, J. C. Moreno, and Y. Amirat, "Lower limb wearable robots for assistance and rehabilitation: A state of the art," *IEEE Syst. J.*, vol. 10, no. 3, pp. 1068–1081, Sep. 2016.

[2] G. S. Sawicki, O. N. Beck, I. Kang, and A. J. Young, "The exoskeleton expansion: Improving walking and running economy," *J. Neuroeng. Rehabil.*, vol. 17, pp. 1–9, 2020.

[3] Z. Lovrenovic and M. Doumit, "Review and analysis of recent development of lower extremity exoskeletons for walking assist," in *Proc. IEEE EMBS Int. Student Conf.*, 2016, pp. 1–4.

[4] A. Otten, C. Voort, A. Stienen, and Aarts, "LIMPACT: A hydraulically powered self-aligning upper limb exoskeleton," *IEEE/ASME Trans. Mechatron.*, vol. 20, no. 5, pp. 2285–2298, Oct. 2015.

[5] V. Arakelian, "Gravity compensation in robotics," *Adv. Robot.*, vol. 30, no. 2, pp. 79–96, 2016.

[6] M. Kolarski and M. Vukobratović, "Dynamic analysis of balanced robot mechanisms," *Mechanism Mach. Theory*, vol. 29, no. 3, pp. 427–454, 1994.

[7] T. Laliberté, C. M. Gosselin, and M. Jean, "Static balancing of 3-dof planar parallel mechanisms," *IEEE/ASME Trans. Mechatron.*, vol. 4, no. 4, pp. 363–377, Dec. 1999.

[8] K. Shi, J. Yang, Z. Hou, and H. Yu, "Design and evaluation of a four-dof upper limb exoskeleton with gravity compensation," *Mechanism Mach. Theory*, vol. 201, 2024, Art. no. 105746.

[9] C.-H. Cho and W. Lee, "Design of a static balancer with equivalent mapping," *Mechanism Mach. Theory*, vol. 101, pp. 36–49, 2016.

[10] C. Cho and S. Kang, "Design of a static balancing mechanism for a serial manipulator with an unconstrained joint space using one-DoF gravity compensators," *IEEE Trans. Robot.*, vol. 30, no. 2, pp. 421–431, Apr. 2014.

[11] Q. Xie, S. Liu, and H. Jiang, "Design of a passive constant-force mechanism based on a five-bar mechanism," *Mechanism Mach. Theory*, vol. 143, 2020, Art. no. 103662.

[12] Y. Liu and D.-p. Yu, "Design of an adjustable cam based constant force mechanism," *Mechanism Mach. Theory*, vol. 103, pp. 85–97, 2016.

[13] P. Wang and Q. Xu, "Design and modeling of constant-force mechanisms: A survey," *Mechanism Mach. Theory*, vol. 119, pp. 1–21, 2018.

[14] K. Koser, "A cam mechanism for gravity-balancing," *Mechan. Res. Commun.*, vol. 36, no. 4, pp. 523–530, 2009.

[15] K. Shi, J. Yang, Y. Tong, and H. Yu, "Design and analysis of a cable-driven gravity compensation mechanism for spatial multi-dof robotic systems," *Mechanism Mach. Theory*, vol. 190, 2023, Art. no. 105452.

[16] R. L. Smith, J. Lobo-Prat, H. van der Kooij, and A. H. Stienen, "Design of a perfect balance system for active upper-extremity exoskeletons," in *Proc. IEEE 13th Int. Conf. Rehabil. Robot.*, 2013, pp. 1–6.

[17] S. K. Agrawal and A. Fattah, "Gravity-balancing of spatial robotic manipulators," *Mechanism Mach. Theory*, vol. 39, no. 12, pp. 1331–1344, 2004.

[18] P.-Y. Lin, W.-B. Shieh, and D.-Z. Chen, "A theoretical study of weight-balanced mechanisms for design of spring assistive mobile arm support (mas)," *Mechanism Mach. Theory*, vol. 61, pp. 156–167, 2013.

[19] Y. Shi, H. Ma, Y. Shao, D. Shi, and W. Zhang, "Design of a passive lower limb exoskeleton with cable-driven remote gravity compensation mechansims," in *Proc. IEEE 18th Conf. Ind. Electron. Appl.*, 2023, pp. 1950–1955.

[20] L. Zhou, W. Chen, W. Chen, and S. Bai, "Design of a passive lower limb exoskeleton for walking assistance with gravity compensation," *Mechanism Mach. Theory*, vol. 150, 2020, Art. no. 103840.

[21] A. Alamdari, R. Haghighi, and V. Krovi, "Gravity-balancing of elastic articulated-cable leg-orthosis emulator," *Mechanism Mach. Theory*, vol. 131, pp. 351–370, 2019.

[22] A. M. Dollar and H. Herr, "Lower extremity exoskeletons and active orthoses: Challenges and state-of-the-art," *IEEE Trans. Robot.*, vol. 24, no. 1, pp. 144–158, Feb. 2008.

[23] D. Shi, W. Zhang, W. Zhang, and X. Ding, "A review on lower limb rehabilitation exoskeleton robots," *Chin. J. Mech. Eng.*, vol. 32, no. 1, pp. 1–11, 2019.

[24] L. W. Lamoreux, "Kinematic measurements in the study of human walking," *Bull Prosthet Res.*, vol. 10, no. 15, pp. 3–84, 1971.

[25] T. Andriacchi and G. Andersson, "A study of lower-limb mechanics during stair-climbing.," *JBJS*, vol. 62, no. 5, pp. 749–757, 1980.

[26] S. E. Chang, T. Pesek, T. R. Pote, J. Hull, J. Geissinger, and Simon, "Design and preliminary evaluation of a flexible exoskeleton to assist with lifting," *Wearable Technol.*, vol. 1, 2020, Art. no. e10.

[27] A. Merlo and I. Campanini, "Applications in movement and gait analysis," in *Proc. Surf. Electromyogr., Physiol., Eng., Appl.*, 2016, pp. 440–459.

[28] T. Rahman et al., "Design and testing of a functional arm orthosis in patients with neuromuscular diseases," *IEEE Trans. Neural Syst. Rehabil. Eng.*, vol. 15, no. 2, pp. 244–251, Jun. 2007.